ACS APPLIED MATERIALS & INTERFACES

Research Article

www.acsami.org

Composition-Driven Phase Boundary and Piezoelectricity in Potassium−Sodium Niobate-Based Ceramics

Ting Zheng, Jiagang Wu,* Dingquan Xiao, and Jianguo Zhu

Department of Materials Science, Sichuan University, Chengdu 610064, P. R. China

Xiangjian Wang and Xiaojie Lou

Multidisciplinary Materials Research Center, Frontier Institute of Science and Technology, and State Key Laboratory for Mechanical Behavior of Materials, Xi'an Jiaotong University, Xi'an 710049, P. R. China

Supporting Information

ABSTRACT: The piezoelectricity of $(K,Na)NbO_3$ ceramics strongly depends on the phase boundary types as well as the doped compositions. Here, we systematically studied the relationships between the compositions and phase boundary types in $(K,Na)(Nb,Sb)O_3-Bi_{0.5}Na_{0.5}AO_3$ (KNNS-BNA, A = Hf, Zr, Ti, Sn) ceramics; then their piezoelectricity can be readily modified. Their phase boundary types are determined by the doped elements. A rhombohedral-tetragonal (R−T) phase boundary can be driven in the compositions range of $0.035 \le$ BNH ≤ 0.040 and $0.035 \le$ BNZ ≤ 0.045; an orthorhombic-tetragonal (O−T) phase boundary is formed in the composition range of $0.005 \le$ BNT ≤ 0.02; and a pure O phase can be only observed regardless of BNS content ($\le$0.01). In addition, the phase boundary types strongly affect their corresponding piezoelectricities. A larger d_{33} (~440−450 pC/N) and a higher d_{33}* (~742−834 pm/V) can be attained in KNNS-BNA (A = Zr and Hf) ceramics due to the involvement of R−T phase boundary, and unfortunately KNNS-BNA (A = Sn and Ti) ceramics possess a relatively poor piezoelectricity ($d_{33} \le 200$ and d_{33}* < 600 pm/V) due to the involvement of other phase structures (O−T or O). In addition, the underlying physical mechanisms for the relationships between piezoelectricity and phase boundary types were also discussed. We believe that comprehensive research can design more excellent ceramic systems concerning potassium−sodium niobate.

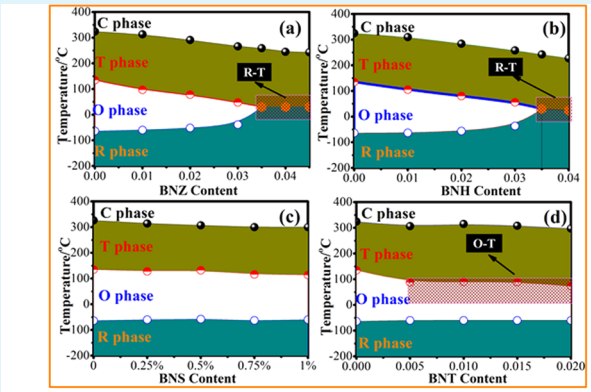

System	d_{33}	strain	d_{33}*	ε_r	tan δ	$\varepsilon_r P_r$	T_C	Phase boundary
BNZ=0.04	440	0.22	742	2067	4.3%	36131	259	R-T
BNH=0.035	450	0.25	834	2192	5.2%	36387	242	R-T
BNS=0.75%	195	0.14	453	678	3.1%	15255	300	O
BNT=0.15	200	0.18	585	592	5.2%	8448	308	O-T

KEYWORDS: *potassium−sodium niobate, composition design, phase boundary type, piezoelectricity, strain*

1. INTRODUCTION

In the past decades, the potassium−sodium niobate ($K_{0.5}Na_{0.5}NbO_3$, KNN) lead-free piezoceramics have attracted a lot of attention because lead-based ($Pb(Zr,Ti)O_3$, PZT) piezoceramics will be finally prohibited in some electronic devices.[1−27] To seek lead-free piezoceramics comparable to PZT, most researchers have tried lots of effective methods such as new preparation technique,[3−5] site engineering,[3,6] addition of second members,[7−9] and the construction of different phase boundaries.[3,6−9] In 2004, Y Saito et al. prepared Li, Ta, and Sb comodified KNN ceramics by the reactive template grain growth method and then obtained a large d_{33} of 416 pC/N by forming orthorhombic-tetragonal (O−T) phase boundary.[3] After that, the construction of phase boundaries by the addition of ions or second members became popular to promote the electrical properties of KNN-based ceramics.[3,6−9,11−19] For example, O−T phase boundary of KNN-based ceramics has been studied widest due to relatively good piezoelectricity,[3,6,9,10] while little attention was given to the construction of rhombohedral−orthorhombic (R−O) phase boundary due to a poor d_{33}.[11] However, the KNN-based ceramics cannot meet the requirements of high performance in some electronic devices by designing two kinds of phase boundaries, especially for the improvement of piezoelectricity. Recently, the breakthrough in

Received: July 6, 2015
Accepted: August 24, 2015
Published: August 24, 2015

DOI: 10.1021/acsami.5b06033
ACS Appl. Mater. Interfaces 2015, 7, 20332−20341

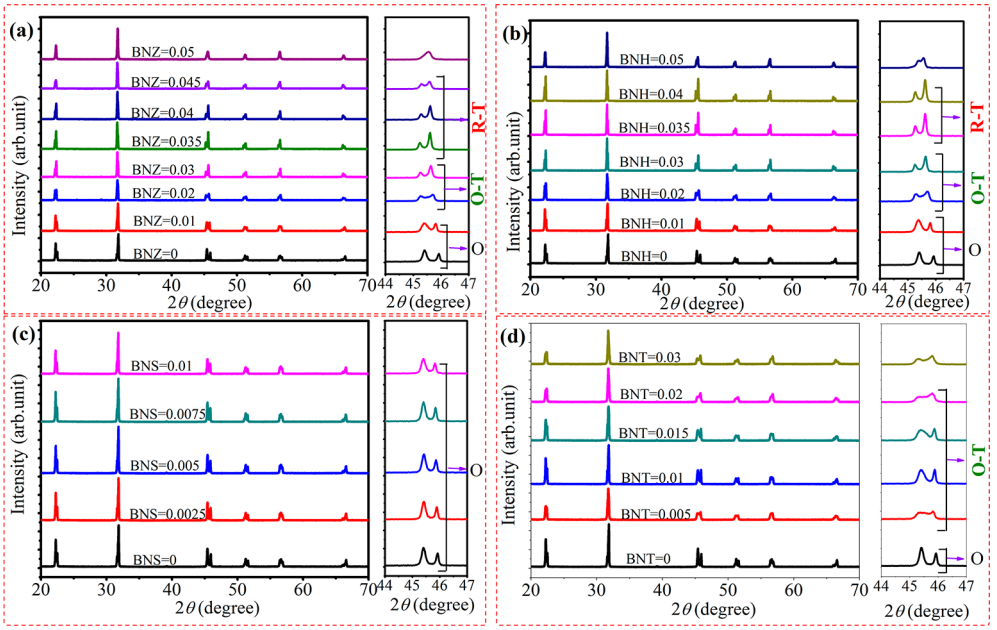

Figure 1. XRD patterns of $(1 - x)$KNNS−xBNA ceramics as a function of (a) BNZ, (b) BNH, (c) BNS, and (d) BNT.

d_{33} has been realized by forming a new phase boundary (e.g., rhombohedral-tetragonal (R−T)), which is superior to these textured KNN-based ceramics.[13,15,17] The research results suggest that the involvement of R−T phase boundary is a key factor to enhance the piezoelectricity of KNN-based ceramics.[12−19] Furthermore, we summarized that the "M" types of (K,Na) $(Nb,Sb)O_3$−$Bi_{0.5}M_{0.5}ZrO_3$ materials seriously affect the piezoelectricity when R−T phase boundary remains unchanged.[18] That is to say, the piezoelectric performance is affected by not only phase boundary types, but also the corresponding composition, and the different doped compositions may cause the variations of phase transition temperatures in KNN-based ceramics.[18] In the past, it was found that the addition of Zr in BMZ can effectively increase T_{R-O} of KNN, and then the combined effects of BMZ can promote the piezoelectric activity of KNN-based ceramics by constructing R−T phase boundary. However, there were few reports on the influences of "A" element types on both phase boundaries and their piezoelectricity in (K,Na) $(Nb,Sb)O_3$−$Bi_{0.5}Na_{0.5}AO_3$ ceramics. In addition, the physical mechanisms for the formation of phase boundaries can be further illuminated if this research can be carried out.

On the basis of the above point of view, we designed $(1 - x)$KNNS−xBNA (A = Hf, Zr, Ti, and Sn) ceramic systems to study the effects of different tetravalent elements (Hf, Zr, Ti, and Sn) on their phase structure and electrical properties in this work. For easy description, we defined $(1 - x)$KNNS−xBNZ, $(1 - x)$KNNS−xBNH, $(1 - x)$KNNS−xBNS, and $(1 - x)$KNNS−xBNT as BNZ, BNH, BNS, and BNT, respectively. Interestingly, the tetravalent elements in BNA strongly affect the phase boundary types of KNNS, and then different piezoelectric activity is induced. Enhanced piezoelectricity can be attained in the composition range of $0.035 \leq \text{BNH} \leq 0.040$ and $0.035 \leq \text{BNZ} \leq 0.045$ owing to the involvement of R−T phase boundary; however, a poor piezoelectricity can be observed in the ceramics modified with BNS and BNT due to the involvement of O phase or O−T phase boundary. As a result, the addition of different tetravalent elements can drive the formation of different phase boundaries, which is the intrinsic reason for their varied piezoelectricity. We believe that this systematic research will point out a clear path for us to obtain high-performance ceramics by constructing R−T phase boundary using appropriate elements.

2. EXPERIMENTAL PROCEDURE

$(1 - x)K_{0.48}Na_{0.52}Nb_{0.96}Sb_{0.04}O_3$−$xBi_{0.5}Na_{0.5}AO_3$ (A = Hf, Zr, Ti, and Sn) piezoceramics have been prepared by the conventional solid state method. Raw materials are listed: K_2CO_3 (99%), Na_2CO_3 (99.8%), Nb_2O_5 (99.5%), Sb_2O_3 (99.99%), Bi_2O_3 (99.999%), SnO_2 (99.8%), ZrO_2 (99%), HfO_2 (99%), and TiO_2 (98%). $NaCO_3$ powders come from Tianjin Institute of Chemical Reagents (China), and other reagents are prepared by Sinopharm Chemical Reagent Co., Ltd. (China). Those powders were weighed and then ball milled for 24 h with alcohol. These dried powders were calcined at 850 °C for 6 h and then mixed with a binder of 8 wt % poly(vinyl alcohol) (PVA). These calcined powders were pressed into the disks with a diameter of 10 mm and a thickness of 1 mm under a pressure of 10 MPa. After PVA was burned off, the $(1 - x)$KNNS−xBNZ and $(1 - x)$KNNS−xBNH samples were sintered at 1075−1100 °C for 3 h in air, the $(1 - x)$KNNS−xBNS samples were sintered at 1075−1090 °C for 3 h in air, and the $(1 - x)$KNNS−xBNT samples were sintered at 1080−1100 °C for 3 h in air. The sintered samples were pasted silver and then fired at 550 °C for 10 min. At last, a direct current electric field of 2−4 kV/mm was applied to pole each sample in a silicon oil bath at 30 °C.

The phase structures of the ceramics were characterized by X-ray diffraction (XRD) (Bruker D8 Advanced XRD, Bruker AXS Inc., Madison, WI, CuKa). The curves of dielectric constant (ε_r) against the temperatures (ε_r−T) of the ceramics were measured by a programmable furnace in connection with LCR analyses (HP 4980, Agilent, USA). HR LabRam Raman spectroscopy system was used to attain the Raman spectra in the temperature range of −100−300 °C, where a 514 nm Ar laser was used for excitation. The field emission-scanning electron microscopy (FE-SEM) (JSM-7500, Japan) was used to observe the surface microstructures of the ceramics with BNZ=0.04, BNH=0.035, BNS=0.0075, and BNT=0.015. Besides, the element mapping of the ceramics with BNZ=0.04, BNH=0.035, BNS=0.0075, and BNT=0.015 were also measured by FE-SEM. P−E hysteresis loops were tested by a Radiant Precision Workstation (USA) with 10 Hz. An impedance analyzer (HP 4294A) was used to test the dielectric properties of each poled sample. In addition, the piezoelectric constant

DOI: 10.1021/acsami.5b06033
ACS Appl. Mater. Interfaces 2015, 7, 20332−20341

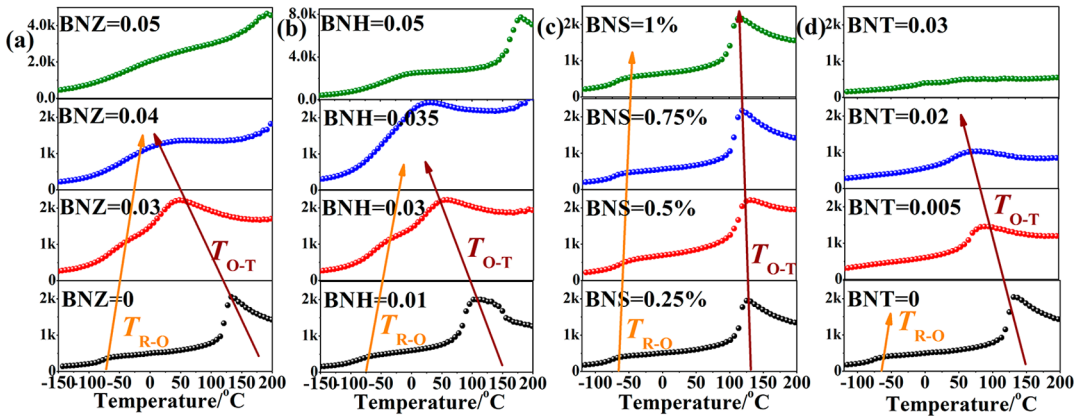

Figure 2. ε_r–T (−150–200 °C) curves of the ceramics as a function of (a) BNZ, (b) BNH, (c) BNS, and (d) BNT.

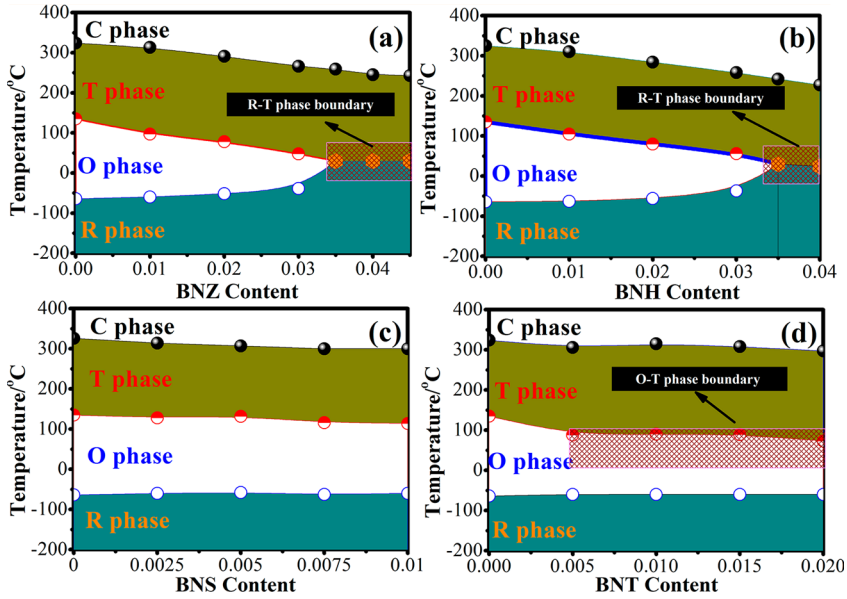

Figure 3. Phase diagrams of the ceramics as a function of (a) BNZ, (b) BNH, (c) BNS, and (d) BNT.

d_{33} and the planar electromechanical coupling factor k_p were tested by piezo-d_{33} meter (ZJ-3 A, China) and impedance analyzer (HP 4194A), respectively. The electric field induced strain was measured by MTI 2000 photonic sensor, and the d_{33}* was calculated by S_{max}/E_{max}. At last, the thermal stability of d_{33} of the ceramics was measured, and the d_{33} was measured at room temperature after the ceramics were annealed in the furnace at various temperatures for 30 min.

3. RESULTS AND DISCUSSION

First, the phase structure of $(1 - x)$KNNS–xBNA (A = Hf, Zr, Ti, and Sn) ceramics will be evaluated by analyzing their XRD patterns, temperature dependence of dielectric constant (ε_r–T), and Raman spectrum. The typical XRD patterns of the ceramics as a function of BNZ, BNH, BNS, and BNT contents, shown in Figure 1, panels a–d, were measured at 20 °C and in the 2θ range of 20–70°. It can be seen from Figure 1 that all the ceramics exhibit a pure ABO_3-type perovskite structure, and no impurity phases can be found. As a result, the Hf, Zr, Ti, and Sn elements can form a stable solid solution with KNNS-BNA. In addition, it can be seen from their respectively amplified XRD profiles, measured in the 2θ range of 43–47°, that the XRD peak shapes are strongly dependent on the corresponding compositions. To further characterize their crystal structures, the ε_r–T curves of the ceramics as a function of BNZ, BNH, BNS, and BNT contents are shown in Figures S1–S4 (Supporting Information), measured in the temperature range of −150–200 °C. As shown in Figure 1, panel a, the XRD peak shapes of the ceramics with BNZ = 0–0.01 match the O phase.[16] Besides, their T_{O-T} (136–99 °C) and T_{R-O} (ca. −60 °C) values are far from room temperature (see Figure S1), providing further evidence for the existence of O phase. A mixed crystal structure can be driven with the increase of BNZ contents (BNZ ≥ 0.02). For example, T_{O-T} (78–47 °C) of the ceramics with BNZ = 0.02–0.03 gradually shifts to room temperature, and their T_{R-O} (ca. −40 °C) value is still far below room temperature (see Figure S1), indicating the involvement of O–T mixed phases. Interestingly, there is only one abnormal dielectric peak in the investigated temperature range for the ceramics with BNZ = 0.035–0.045, showing that the R–T phase boundary can be driven to room temperature. Finally, there is a shoulder for the ε_r–T curves of the ceramics with BNZ = 0.05, that is, a suppressed R–T phase boundary gradually appears. As a result, there is an O phase for BNZ = 0–0.01, O–T phase boundary for BNZ = 0.02–0.03, R–T phase boundary for BNZ = 0.035–0.045, and a suppressed R–T phase boundary for BNZ = 0.05. By using the same analysis method (see Figures 1b and S2), there is a similar phase

DOI: 10.1021/acsami.5b06033
ACS Appl. Mater. Interfaces 2015, 7, 20332–20341

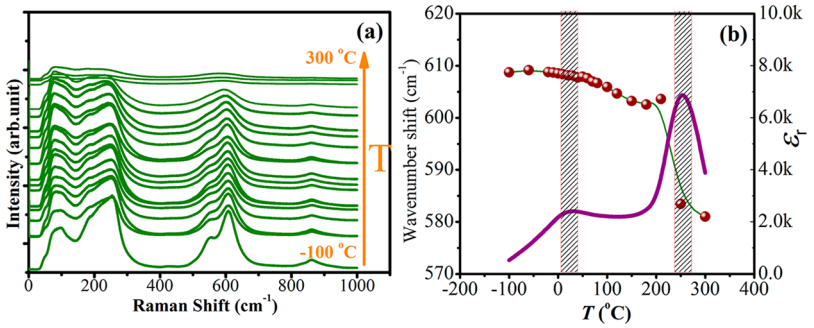

Figure 4. (a) Temperature dependence of Raman spectra for 0.965KNNS-0.035BNH. (b) Evolution of the ν_1 mode and dielectric permittivity results of the 0.965KNNS-0.035BNH ceramics as a function of temperature ranging from −100−300 °C.

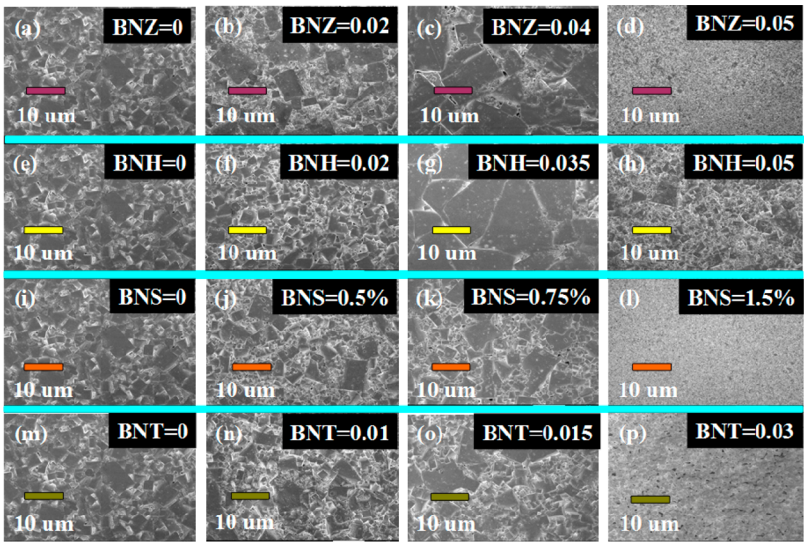

Figure 5. FE-SEM images of surface morphologies in the ceramics with (a−d) BNZ = 0, 0.02, 0.04, 0.05; (e−h) BNH = 0, 0.02, 0.035, 0.05; (i−l) BNS = 0%, 0.5%, 0.75%, 1.5%; and (m−p) BNT = 0, 0.01, 0.015, 0.03.

transition with varied compositions for the ceramics modified with BNH. However, their T_{O-T} and T_{R-O} values of the ceramics with BNS = 0−1% almost remain unchanged (see Figure S3), and T_{R-O} is seriously suppressed with the addition of BNT (see Figure S4). To clearly and intuitively compare the changed trends of phase structure, we selected the ε_r-T curves of four components (BNZ, BNH, BNS, and BNT) to show the variations of both T_{O-T} and T_{R-O}, as shown in Figure 2. It is clearly pointed out that the addition of BNZ and BNH decreases T_{O-T} and increases T_{R-O} simultaneously, which results in the formation of R−T phase boundary (see Figure 2a,b). However, the addition of BNS almost has no effects on their T_{O-T} and T_{R-O} values, which leads to the appearance of O phase at room temperature (see Figure 2c). More interestingly, the addition of BNT not only decreases T_{O-T}, but also seriously suppresses T_{R-O} (see Figure 2d). Recent studies have shown that the addition of BNT will decrease T_C and T_{O-T} of KNN-based ceramics along with the appearance of the diffuse phase transition.[24,25] As a result, different crystal structures can be driven by the addition of different elements (Hf, Zr, Ti, and Sn). Figure 3, panels a−d show the phase diagrams of the ceramics as a function of BNZ, BNH, BNS, and BNT contents. It should be highlighted that their T_C values are derived from their corresponding ε_r-T curves, measured at 100 kHz and T = 25−450 °C, as shown in Figure S5 (Supporting Information). In addition, the values of T_{O-T} and T_{R-O} are also derived from their corresponding ε_r-T curves, measured at 100 kHz and T = −150−200 °C, as shown in Figures S1−S4 (Supporting Information). As shown in Figure 3, panels a and b, the addition of BNZ and BNH can linearly reduce T_C, and the O phase is suppressed gradually with the increase of BNZ or BNH contents, along with the increase of T_{R-O} and the decrease of T_{O-T}. Finally, the O phase can be completely suppressed, and then the R−T phase boundary can be driven in the composition ranges of $0.035 \leq \text{BNZ} \leq 0.045$ and $0.035 \leq \text{BNH} \leq 0.04$. However, the addition of BNS and BNT can construct different phase diagrams, as shown in Figure 3, panels c and d. It can be seen from Figure 3, panel c that the BNS almost has no effects on T_{O-T} and T_{R-O} of KNNS, and T_C is only slightly reduced in the composition range of 0−0.01. Thus, a pure O phase is formed in the ceramics by doping different BNS contents. Finally, the doping with BNT can not only decrease T_{O-T}, but also seriously suppress T_{R-O} of KNNS, as discussed earlier. At the same time, the O−T phase coexistence with BNT ≥ 0.005 is clearly shown in Figures 1, panel d, and 3, panel d. Therefore, we can conjecture that O−T phase boundary can be driven in KNNS-BNT ceramics with the composition range of 0.005−0.02 even if their T_{R-O} values cannot be detected according to their ε_r-T curves.

To further confirm the phase structure, we have measured the temperature-dependent Raman spectrum of 0.965KNNS-0.035BNH ceramics from 0−1000 cm^{-1}, as shown in Figure 4,

DOI: 10.1021/acsami.5b06033
ACS Appl. Mater. Interfaces 2015, 7, 20332−20341

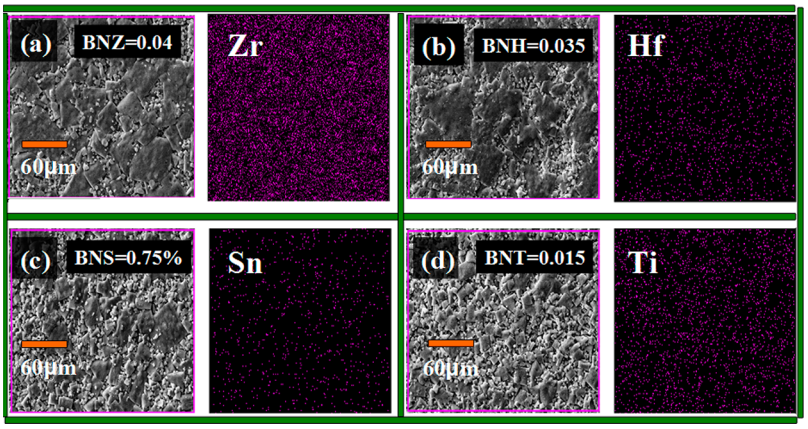

Figure 6. Zr, Hf, Sn, and Ti mapping of the surface in the ceramics with (a) BNZ = 0.04, (b) BNH = 0.035, (c) BNS = 0.75%, and (d) BNT = 0.015.

panel a. As reported in our previous results, the stronger υ_1 mode (~600 cm^{-1}) and the weaker υ_2 mode (~550 cm^{-1}) are related to the variation of NbO_6 octahedral, and thus the two modes can be used to characterize the phase transitions.[19] With the increase of temperatures, the υ_1 mode shifts to a lower wavenumber, and the υ_2 mode gradually disappears. The temperature dependence of the υ_1 mode and dielectric permittivity of the ceramics were included in Figure 4, panel b. We can see that the two anomalies in temperature-dependent υ_1 mode curves correspond to their T_{R-T} and T_C values in temperature-dependent dielectric constant curves. As a result, the existence of R−T phase boundary in 0.965KNNS-0.035BNH ceramics is further confirmed.

Due to the differences in microstructure can affect functional properties of ceramics,[31] the FE-SEM images of surface morphologies of the ceramics as a function of BNZ = 0, 0.02, 0.04, 0.05; BNH = 0, 0.02, 0.035, 0.05; BNS = 0%, 0.5%, 0.75%, 1.5%; and BNT = 0, 0.01, 0.015, 0.03 have been shown in Figure 5. As shown in Figure 5, panels a−c, a typical bimodal grain size distribution was observed in the ceramics with BNZ ≤ 0.04, and moreover a dense microstructure was also developed. Besides, the large grains become larger with the increase of BNZ contents, while the grain sizes refine shapely when BNZ contents reach 0.05 (see Figure 5d), which can be used to explain the degradation of electrical properties of the ceramics with excessive BNZ contents. We can find from Figure 5, panels e−p that the microstructure evolutions of the ceramics with different BNH, BNS, and BNT contents are almost similar to those of the ones with different BNZ contents, indicating that the amount of dopants affects the microstructure seriously. On the other hand, we compared the FE-SEM images of surface morphologies of the ceramics as a function of BNZ = 0.04, BNH = 0.035, BNS = 0.75%, and BNT = 0.015 (see Figure 5c,g,k,o), where a high d_{33} can be shown in these ceramics for a given material system. It can be also found that abnormal grains can be shown in the ceramics with BNZ and BNH with respect to that of BNS or BNT-doped ones. For the addition of BNH or BNZ, abnormal grain growths will promote the piezoelectric properties of KNN-based ceramics. To further analyze the elements distributions, we characterized the Zr, Hf, Sn, and Ti distributions of these ceramics. Figure 6, panels a−d, respectively, show the elements mapping of surface morphologies of the ceramics with BNZ = 0.04, BNH = 0.035, BNS = 0.75%, and BNT = 0.015, characterized by the energy-dispersive X-ray analysis. A homogeneous elements distribution can be observed in four kinds of the ceramics. As a result, the doping with different elements (Hf, Zr, Ti, and Sn) does not cause the variations of element distributions in this work.

Figure 7 shows the ferroelectricity of four kinds of the ceramics measured at room temperature and 10 Hz. Figure 7,

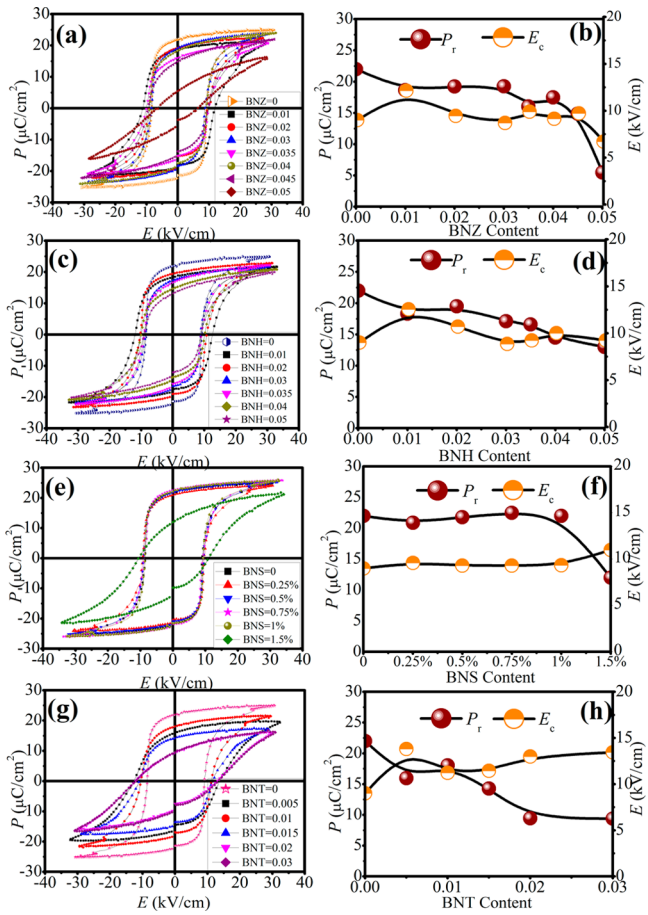

Figure 7. (a, c, e, g) *P*−*E* loops of the ceramics as a function of BNZ, BNH, BNS, and BNT content; (b, d, f, h) respective P_r and E_C against BNZ, BNH, BNS, and BNT content.

panels a, c, e, and g, respectively, show the *P*−*E* loops of the ceramics with BNZ, BNH, BNS, and BNT contents measured at room temperature and *f* = 10 Hz. It can be seen that all the samples possess a typical *P*−*E* loop, while their ferroelectricity is also strongly dependent on the kind of material as well as the

DOI: 10.1021/acsami.5b06033
ACS Appl. Mater. Interfaces 2015, 7, 20332−20341

Table 1. Relationships between Electrical Properties and Phase Boundary Types in the KNNS-BNA Ceramics

system	d_{33} (pC/N)	k_p	strain	d_{33}* (pm/V)	Pr (μC/cm^2)	E_C (kV/cm)	ε_r	tan δ	$\varepsilon_r P_r$	Tc (°C)	phase boundary
BNZ=0.04	440	0.48	0.22	742	17.48	9.15	2067	4.3%	36131	259	R−T
BNH=0.035	450	0.49	0.25	834	16.60	9.23	2192	5.2%	36387	242	R−T
BNS=0.75%	195	0.53	0.14	453	22.50	9.30	678	3.1%	15255	300	O
BNT=0.15	200	0.41	0.18	585	14.27	11.44	592	5.2%	8448	308	O−T

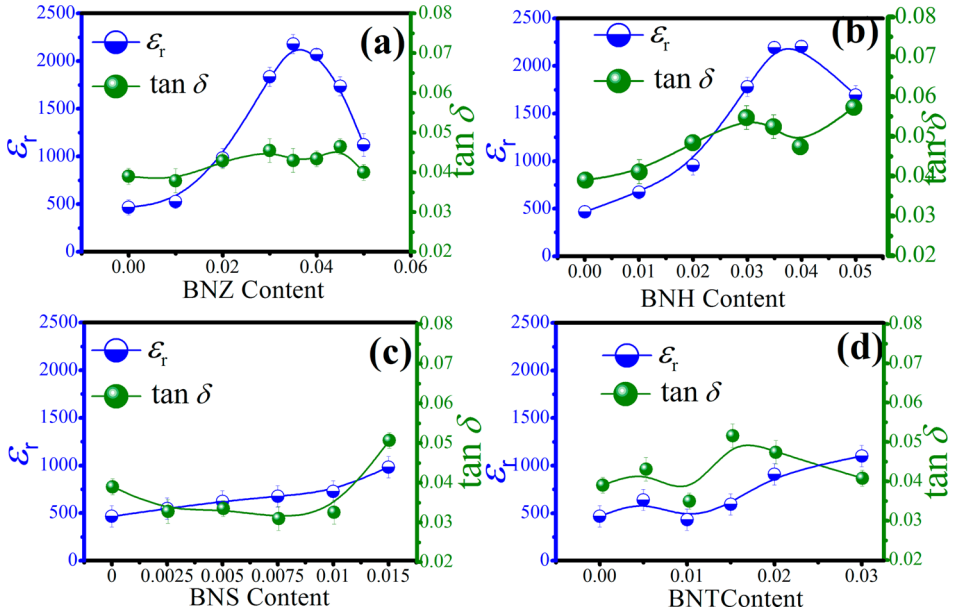

Figure 8. (a−d) ε_r and tan δ of the ceramics as a function of BNZ, BNH, BNS, and BNT contents, respectively.

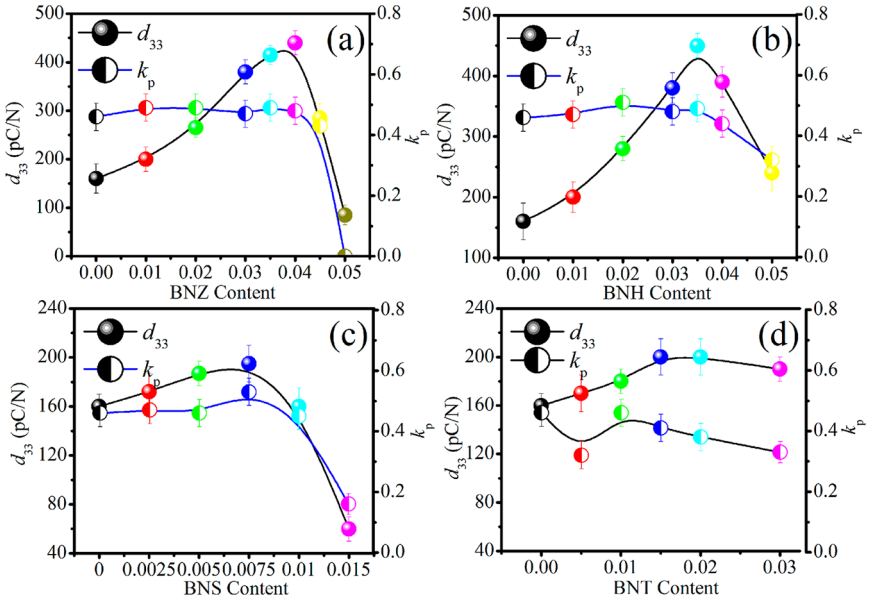

Figure 9. d_{33} and k_p values of the ceramics as a function of (a) BNZ, (b) BNH, (c) BNS, and (d) BNT contents.

corresponding compositions. To clearly find out the effects of BNZ, BNH, BNS, and BNT contents on the ferroelectricity, remnant polarization (P_r) and coercive field (E_C) derived from the corresponding P−E loops were shown in Figure 7, panels b, d, f, and h. It can be clearly found that P_r gradually decreases with the increase of BNZ, BNH, and BNT contents, as shown in Figure 7, panels b, d, and h. However, BNS shows different effects on P_r, that is, there is almost no change in the P_r for the compositions range of 0−1%, and then P_r drops for BNS = 1.5%, as shown in Figure 7, panel f. Table 1 summarizes the relationships between phase boundary types and electrical properties of the ceramics with BNZ = 0.04, BNH = 0.035, BNS = 0.75%, and BNT = 0.015, where a higher d_{33} can be shown. As shown in Table 1, we can identify the influences of different doped elements on their electrical properties. One can see that different phase boundaries strongly affect the ferroelectric properties of the ceramics. The ceramics with O phase (e.g., the doping with BNS) possess a highest P_r value

DOI: 10.1021/acsami.5b06033
ACS Appl. Mater. Interfaces 2015, 7, 20332−20341

among all the ceramics. According to the development of KNN-based ceramics, the addition of ions or ABO_3 will inevitably decreases P_r with the respect to a pure KNN ceramic.[13,19,21] It is of interest to note that a higher P_r value can be attained in the ceramics with BNS < 0.015. However, the ceramics with O−T or R−T possess a similar P_r value, and their E_C values are slightly affected by the phase boundary types. As a result, it is difficult to improve the ferroelectricity of KNN-based ceramics by the construction of phase boundaries due to the addition of some elements (e.g., Sb).[30]

Figure 8, panels a−d, respectively, show the ε_r and tan δ of the ceramics as a function of BNZ, BNH, BNS, and BNT contents measured at room temperature and f = 100 kHz. As shown in Figure 8, panels a and b, ε_r increases gradually and then drops with the increase of BNZ or BNH contents, reaching a maximum value in the region of R−T phase boundary. We can see that their tan δ is limited from 0.03−0.06 under the investigated composition range. However, ε_r of the ceramics with BNS and BNT exhibits different changing trends as compared with those of the ones doped with BNZ and BNH, that is, ε_r increases continuously with increasing BNS and BNT contents, and the values of ε_r are in the range of 400−1100, as shown in Figures 8, panels c and d. Table 1 shows the dielectric properties of the ceramics with BNZ = 0.04, BNH = 0.035, BNS = 0.75%, and BNT = 0.015. The ε_r value of the ceramics with BNH and BNZ is three-times higher than the ones with BNS and BNH. In addition, BNZ and BNH have the same impact on ε_r, and a relatively high ε_r value (>2000) can be obtained in the R−T phase boundary. In the past, it was well understood that there is a close relationship between ε_r and d_{33} of a material,[15,19] that is, a higher ε_r is proportional to the d_{33}.

In the past, we have systematically analyzed the role of phase boundary types in the improved piezoelectricity for KNN-based ceramics.[17] In this part, we identified the relationships between piezoelectricity and phase boundary types using the KNNS-BNA ceramics materials. The piezoelectricity of the ceramics with different BNZ, BNH, BNS, and BNT contents was shown in Figure 9, panels a−d. One can see that d_{33} first increases and then decreases, reaching a maximum value (~440−450 pC/N) for BNZ = 0.04 and BNH = 0.035 due to the involvement of R−T phase boundary, as shown in Figure 9, panels a and b. In addition, a higher d_{33} can be observed in the ceramics with optimum BNS or BNT contents. However, d_{33} values of the ceramics are strongly dependent on the phase boundary types. We can see that d_{33} values of the ceramics with BNS and BNT are much lower than those of the ones with BNZ or BNH because of the involvement of different phase boundaries, which is similar to the variations of dielectric properties. Therefore, it is not wise to choose tetravalent elements (Sn or Ti) to completely replace A site of KNNS-BNA to promote their piezoelectricity due to the absence of R−T phase boundary. However, this is not to say that the addition of Sn or Ti will absolutely deteriorate electrical properties of KNN. For example, previous research has revealed that the Sn or Ti part substitutions for Zr can help enhance the piezoelectricity of KNN-based ceramics.[19,26,28] Interestingly, there is a similar changing trend of phase structure and electrical properties of the ceramics with BNZ or BNH, indicating that the Zr and Hf elements have the same effect on crystal structure and electrical properties of KNN-based ceramics. However, we also found that a low Hf content can drive the formation of R−T phase boundary, and then a slightly higher d_{33} can be attained in this ceramic system (see Table 1). The results show that the piezoelectric properties of KNNS-BNA ceramics can be enhanced by doping not only by Zr, but also byHf.

In the past, we also found that the strain of KNN-based ceramics is also related to phase boundaries.[18,19] Figure 10,

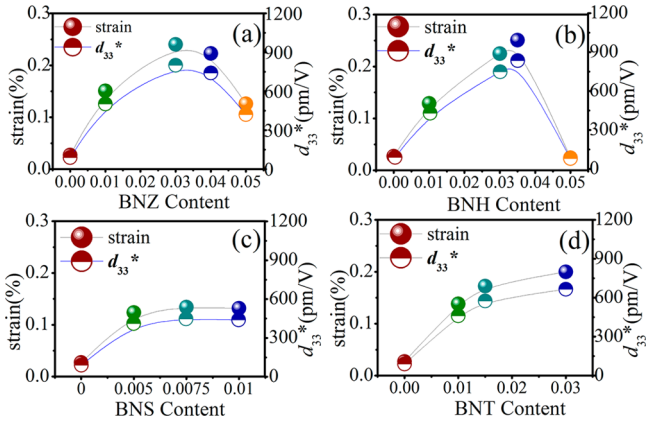

Figure 10. Strain and d_{33}* of the ceramics as a function of (a) BNZ, (b) BNH, (c) BNS, and (d) BNT contents.

panels a−d show the composition dependence of strain and d_{33}* (d_{33}* = S_{max}/E_{max}) of the ceramics with BNZ, BNH, BNS, and BNT contents, whose data were derived from the strain−field curves, as shown in Figure S6 (Supporting Information). Both strain and d_{33}* exhibit a similar changing trend in the investigated composition range, and then the addition of BNZ, BNH, BNS, or BNT can improve the strain to a certain extent. As shown in Figure 10, panels a and b, both strain and d_{33}* first increase and then decrease with the increase of BNZ and BNH contents. Interestingly, this changing trend is also similar to those of d_{33} or ε_r. Large d_{33}* of 742 pm/V and 835 pm/V can be attained in 0.96KNNS-0.04BNZ and 0.965KNNS-0.035BNH ceramics, respectively. As shown in Figure 10, panel c, the strain value maintains a relatively stable value (0.12%−0.14%) in the BNS composition range of 0.5−1%. However, it was found from Figure 10, panel d that the strain value increases continuously with the increase of BNT contents. As a result, different elements (Zr, Hf, Sn, and Ti) affect the strain behavior of the ceramics. The multiphase coexistence can help promote the strain values of KNN-based ceramics, that is, the ceramics with O phase possess a lower strain value with respect to the ones with O−T and R−T. In addition, both BNZ and BNH have the same impact on strain properties of KNN-based ceramics, and a relatively high strain value can be simultaneously obtained in R−T phase boundary. As a result, this result confirmed that the construction of phase boundaries can effectively promote the strain behavior of KNN-based ceramics. Previously, it was reported that the electric field-induced strain for a ferroelectric material mainly originated from the switching of non-180° domain contribution.[27−29] In this work, a high strain value can be obtained in BNZ- and BNH-modified ceramics due to the easy switching of non-180° domain because their R−T phase boundary is near the room temperature. We can conjecture that the low strain values obtained in the BNS-doped ceramics can be attributed to the absence of phase boundaries. At last, the BNT can improve strain value to a certain extent partly due to the involvement of O−T phase boundary.

Liang et al. calculated and discussed the piezoelectric anisotropy and found its change with temperature in alkali

DOI: 10.1021/acsami.5b06033
ACS Appl. Mater. Interfaces 2015, 7, 20332−20341

niobates.[32] However, it was hard to realize the measurement about temperature stability of d_{33} in our group. For practical application, the thermal stability of d_{33} is also very important. Figure 11, panels a–d show the thermal stability of d_{33} in the ceramics as a function of BNZ, BNH, BNS, and BNT contents, where d_{33} was tested at room temperature after the samples were annealed in the furnace at various temperatures for 30 min. It can be seen that the thermal stability of d_{33} curves is strongly dependent on the material systems and compositions. For example, the thermal stability of the ceramics with BNZ is almost similar to that of the ones with BNH content, as shown in Figure 11, panels a and b. For the ceramics with BNZ = 0–0.01 or BNH = 0–0.01, relatively stable thermal stability behavior can be found, which may be due to the involvement of O phase.[20] With the increase of BNZ or BNH contents, the d_{33} decreases slowly due to the formation of phase boundary with the increase of annealing temperature (T_a) and then drops quickly when T_a is close to T_C. In our previous work, we have studied the effects of BNZ content on the thermal stability of KNN-based ceramics,[21] and a similar phenomenon appears in this work. However, a relatively good d_{33} (~330 pC/N) value can still be maintained for the ceramics with the highest d_{33} (~440 pC/N) when T_a is near T_C. In addition, for the ceramics with BNS, we can find that a relatively stable thermal stability properties of d_{33} can be achieved except for BNS = 1.5%. The previous studies show that the O phase is helpful to promote the thermal stability of KNN-based ceramics,[20] and thus a relatively good thermal stability can appear in the KNNS-BNS ceramics. For BNT-modified KNN ceramics, the d_{33} value reduces slowly with the increase of T_a. It was reported that the d_{33} value of KNLN6–0.03BNT ceramics is nearly temperature independent in the range from room temperature to 380° because the phase transition temperature is shifted to below room temperature.[22] Besides, in KNN-BNKLZ–xBNT ceramic system, the normalized d_{33} still can be maintained at more than 80%; the results are similar to the results of our experiment.[23] The inset in Figure 9, panel d shows the composition dependence of the thermal stability of the ceramics with BNZ = 0.04, BNH = 0.035, BNS = 0.75%, and BNT = 0.015. We found that the ceramics with O phase show a better thermal stability as compared with the ones with other phase structure, a poorer thermal stability was observed in the ceramics with O–T, and the ceramics with R–T possess a similar thermal stability. As confirmed by others, the O phase will promote the thermal stability of the d_{33} in KNN-based ceramics, but a low d_{33} cannot benefit its practical applications. In this work, a high d_{33} value of 350 pC/N (T = 200 °C) can be well maintained in R–T ceramics, although a relatively weak thermal stability is shown.

In this section, we discussed the relationships among electrical properties, phase boundary types, and compositions through four kinds of material systems. Table 1 lists the relationships between electrical properties and phase boundary types of the ceramics with BNZ = 0.04, BNH = 0.035, BNS = 0.75%, and BNT = 0.015. First, we analyzed the physical

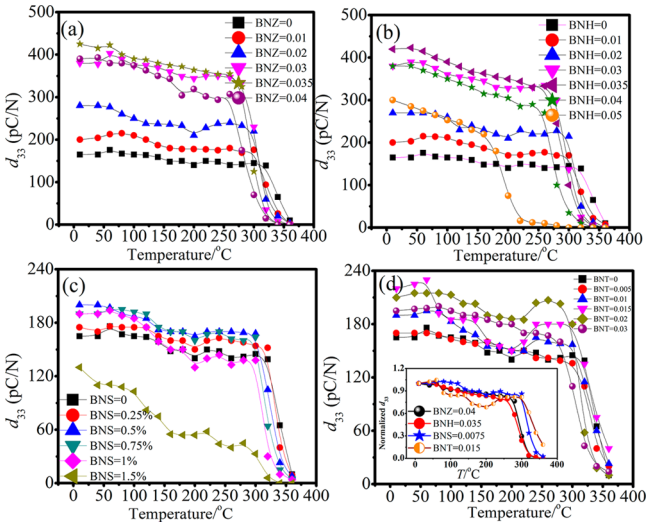

Figure 11. d_{33} versus annealing temperature of the ceramics with (a) BNZ, (b) BNH, (c) BNS, and (d) BNT contents. The inset in panel d is the composition dependence of the thermal stability.

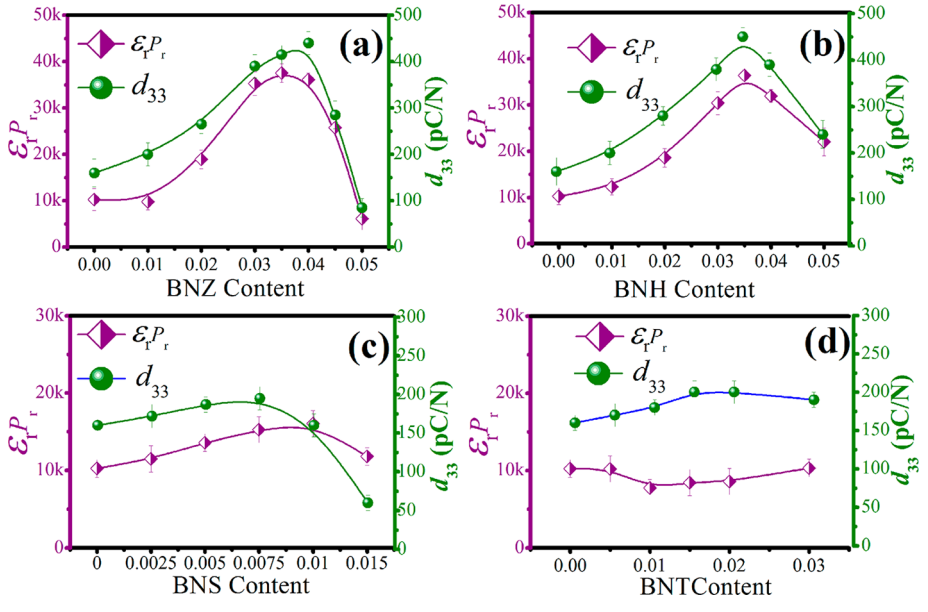

Figure 12. d_{33} versus $\varepsilon_r P_r$ of the ceramics with (a) BNZ, (b) BNH, (c) BNS, and (d) BNT contents.

DOI: 10.1021/acsami.5b06033
ACS Appl. Mater. Interfaces 2015, 7, 20332–20341

mechanisms for the enhanced piezoelectric properties. The piezoelectricity has a close relationship with the phase boundary types of KNN-based ceramics. A much larger d_{33} (~440−450 pC/N) value can be obtained by constructing the R−T phase boundary, while a poorer d_{33} value appears in the pure O phase or O−T phase boundary. Therefore, a high d_{33} value of the ceramics with BNZ or BNH is mainly assigned to the R−T phase boundary.[12,15,18,19] Besides, the d_{33} value is also related to both ferroelectric and dielectric properties of a material.[13] Thus, we show the curves of both d_{33} and $\varepsilon_r P_r$ versus BNZ, BNH, BNS, and BNT contents, as shown in Figure 12. It can be seen that the changing trend of d_{33} is similar to that of $\varepsilon_r P_r$, indicating that the enhanced d_{33} is partly due to the increase of $\varepsilon_r P_r$. Second, it was clearly found that there is a contradiction between d_{33} and T_C. For example, a large d_{33} (~440−450 pC/N) value can be achieved in the ceramics with BNZ = 0.04 or BNH = 0.035, while a low T_C (242 or 259 °C) value appears. There is a lower d_{33} value associated with a higher T_C (~300 °C) value for the ceramics with BNS = 0.75% or BNT = 0.015. Third, the addition of different elements (Hf, Zr, Ti, and Sn) drives different phase boundaries of KNN-based ceramics. Both BNZ and BNH can increase T_{R-O} and decrease T_{O-T} of KNN ceramics simultaneously, resulting in the formation of R−T phase boundary.[21] However, a pure O phase can be well maintained because the BNS almost has no effect on T_{R-O} and T_{O-T}. Although the BNT can decreases T_{O-T} of KNN, the phase transition is gradually suppressed especially for the R−O phase transition,[22,24−26] which leads to the formation of O−T phase boundary instead of R−T phase boundary. That is to say, different elements (Hf, Zr, Ti, and Sn) result in the formation of different phase boundaries because of their different effects on the phase transition temperature and then cause the variations of electrical properties. As a result, the comprehensive and comparative studies of four ceramic systems can point out a way to further promote the piezoelectric activity by constructing different phase boundaries using different elements (e.g., Hf, Zr, Ti, and Sn). Most importantly, the earlier mentioned results tell us that the Hf element has the same function to Zr for KNNS-BNA material system, while the Hf-doped KNN-based ceramics did not attract attention in the past. Therefore, the researches about Hf -doped KNN ceramics may become a new hot spot.

4. CONCLUSION

In this work, our objective is to design the $(1-x)$KNNS−xBNA (A = Hf, Zr, Ti, and Sn) ceramic system to study the effects of BNZ, BNH, BNS, and BNT contents on their phase structure and electrical properties. The results showed that the Zr and Hf elements have the same function on the construction of phase boundaries and electrical properties. Large d_{33} (~440−450 pC/N) and d_{33}* (~742−834 pm/V) values have been obtained in the KNNS-0.04BNZ or KNNS-0.035BNH ceramics with R−T phase boundary, indicating that the Zr or Hf doping will be effective to enhance the electrical properties of KNN-based ceramics. However, a poor piezoelectricity is attained in the ceramics with BNS or BNT content due to the absence of R−T phase boundary. As a result, the comprehensive and comparative research clarified the role of different tetravalent elements (Zr, Hf, Sn, Ti) on both the construction of phase boundary and the variations of electrical properties in KNN-based ceramics.

■ ASSOCIATED CONTENT

Supporting Information

The Supporting Information is available free of charge on the ACS Publications website at DOI: 10.1021/acsami.5b06033.

Temperature dependence of dielectric constant and strain hysteresis (PDF)

■ AUTHOR INFORMATION

Corresponding Author

*E-mail: wujiagang0208@163.com and msewujg@scu.edu.cn.

Notes

The authors declare no competing financial interest.

■ ACKNOWLEDGMENTS

The authors gratefully acknowledge the support of the Fundamental Research Funds for the Central Universities (2012SCU04A01), the National Science Foundation of China (NSFC Nos. 51102173, 51272164, 51332003, and 51472169), and the College of Materials Science and Engineering of Sichuan University. We thank Hui Wang for measuring the SEM images.

■ REFERENCES

(1) Jaffe, B.; Cook, W. R.; Jaffe, H. *Piezoelectric Ceramics*; Academic New York: New York, 1971.

(2) Shrout, T. R.; Zhang, S. J. Lead-free Piezoelectric Ceramics: Alternatives for PZT? *J. Electroceram.* **2007**, *19*, 111.

(3) Saito, Y.; Takao, H.; Tani, T.; Nonoyama, T.; Takatori, K.; Homma, T.; Nagaya, T.; Nakamura, M. Lead-free Piezoceramics. *Nature* **2004**, *432*, 84.

(4) Haertling, G. H. Properties of Hot-pressed Ferroelectric Alkali Niobate Ceramics. *J. Am. Ceram. Soc.* **1967**, *50*, 329−330.

(5) Li, J. F.; Wang, K.; et al. Ferroelectric and Piezoelectric Properties of Fine-Grained $(K_{0.5}Na_{0.5})NbO_3$ Lead-free Piezoelectric Ceramics Prepared by Spark Plasma Sintering. *J. Am. Ceram. Soc.* **2006**, *89* (2), 706−709.

(6) Hollenstein, E.; Davis, M.; Damjanovic, D.; Setter, N. Piezoelectric Properties of Li- and Ta-Modified $(K_{0.5}Na_{0.5})NbO_3$ Ceramics. *Appl. Phys. Lett.* **2005**, *87*, 182905.

(7) Lei, C.; Ye, Z. G. Lead-free Piezoelectric Ceramics Derived from the $K_{0.5}Na_{0.5}NbO_3$−$AgNbO_3$ Solid Solution System. *Appl. Phys. Lett.* **2008**, *93*, 042901.

(8) Guo, Y. P.; Kakimoto, K.; Ohsato, H. Phase Transitional Behavior and Piezoelectric Properties of $(Na_{0.5}K_{0.5})NbO_3$−$LiNbO_3$ Ceramics. *Appl. Phys. Lett.* **2004**, *85*, 4121.

(9) Wang, K.; Li, J. F.; Zhou, J. J. High Normalized Strain Obtained in Li-Modified $(K,Na)NbO_3$ Lead-free Piezoceramics. *Appl. Phys. Express* **2011**, *4*, 061501.

(10) Akdoğan, E. K.; Kerman, K.; Abazari, M.; Safari, A. Origin of High Piezoelectric Activity in Ferroelectric $(K_{0.44}Na_{0.52}Li_{0.04})$?$(Nb_{0.84}Ta_{0.1}Sb_{0.06})O_3$ Ceramics. *Appl. Phys. Lett.* **2008**, *92* (11), 112908.

(11) Zuo, R. Z.; Fu, J.; Lv, D. Y.; Liu, Y. Antimony Tuned Rhombohedral-Orthorhombic Phase Transition and Enhanced Piezoelectric Properties in Sodium Potassium Niobate. *J. Am. Ceram. Soc.* **2010**, *93* (9), 2783.

(12) Zuo, R. Z.; Fu, J. Rhombohedral−Tetragonal Phase Coexistence and Piezoelectric Properties of (NaK) $(NbSb)O_3$−$LiTaO_3$−$BaZrO_3$ Lead-free Ceramics. *J. Am. Ceram. Soc.* **2011**, *94*, 1467.

(13) Zhang, B. Y.; Wu, J. G.; Cheng, X. J.; Wang, X. P.; Xiao, D. Q.; Zhu, J. G.; Wang, X. J.; Lou, X. J. Lead-free Piezoelectrics Based on Potassium−Sodium Niobate with Giant d_{33}. *ACS Appl. Mater. Interfaces* **2013**, *5* (16), 7718.

(14) Liang, W. F.; Wu, W. J.; Xiao, D. Q.; Zhu, J. G.; Wu, J. G. Construction of New Morphotropic Phase Boundary in 0.94-

DOI: 10.1021/acsami.5b06033
ACS Appl. Mater. Interfaces 2015, 7, 20332−20341

($K_{0.42-x}Na_{0.6}Ba_xNb_{1-x}Zr_x$)$O_3-0.06LiSbO_3$ Lead-free Piezoelectric Ceramics. *J. Mater. Sci.* **2011**, *46*, 6871.
(15) Wang, X.; Wu, J.; Xiao, D.; Zhu, J.; Cheng, X.; Zheng, T.; Zhang, B.; Lou, X.; Wang, X. Giant Piezoelectricity in Potassium−Sodium Niobate Lead-free Ceramics. *J. Am. Chem. Soc.* **2014**, *136* (7), 2905.
(16) Cheng, X. J.; Wu, J. G.; Wang, X. P.; Zhang, B.; Zhu, J. G.; Xiao, D. Q.; Wang, X.; Lou, X. Giant d_{33} in (K,Na) (Nb,Sb)O_3-(Bi,Na,K,Li)ZrO_3 Based Lead-free Piezoelectrics with High T_C. *Appl. Phys. Lett.* **2013**, *103*, 052906.
(17) Wu, J. G.; Xiao, D. Q.; Zhu, J. G. Potassium−Sodium Niobate Lead-free Piezoelectric Materials: Past, Present, and Future of Phase Boundaries. *Chem. Rev.* **2015**, *115* (7), 2559−2595.
(18) Zheng, T.; Wu, J.; Xiao, D.; Zhu, J.; Wang, X.; Lou, X. Potassium-Sodium Niobate Lead-free Ceramics: Modified Strain as well as Piezoelectricity. *J. Mater. Chem. A* **2015**, *3*, 1868.
(19) Zheng, T.; Wu, J.; Xiao, D.; Zhu, J.; Wang, X.; Xin, L.; Lou, X. Strong Piezoelectricity in (K,Na) (Nb,Sb)O_3-(Bi,K) (Zr,Sn)O_3 Lead-free Binary System: Identification and Role of Multiphase Coexistence. *ACS Appl. Mater. Interfaces* **2015**, *7* (10), 5927−5937.
(20) Gao, Y.; Zhang, J. L.; Zong, X. J.; Wang, C. L.; Li, J. C. Extremely Temperature-Stable Piezoelectric Properties of Orthorhombic Phase in (K,Na)NbO3-Based Ceramics. *J. Appl. Phys.* **2010**, *107*, 074101.
(21) Zheng, T.; Wu, J.; Cheng, X.; Wang, X.; Zhang, B.; Xiao, D.; Zhu, J.; Wang, X.; Lou, X. Giant Piezoelectricity and Large Electric Field -induced Strain in (1-x)($K_{0.4}Na_{0.6}$) ($Nb_{0.955}Sb_{0.045}$)O_3-$x$$Bi_{0.5}Na_{0.5}ZrO_3$ Lead-free Ceramics. *J. Mater. Chem. C* **2014**, *2*, 8796.
(22) Hao, J. G.; Xu, Z. J.; Chu, R. Q.; Zhang, Y. J.; Chen, Q.; Li, W.; Fu, P.; Zang, G. Z.; Li, G. R.; Yin, Q. R. Enhanced Temperature Stability of (1-x)$(K_{0.5}Na_{0.5})_{0.94}Li_{0.06}NbO_3$-$x$$(Bi_{0.5}Na_{0.5})TiO_3$ Lead-free Piezoelectric Ceramics. *J. Electron. Mater.* **2010**, *39*, 347−354.
(23) Cheng, X. J.; Wu, J. G.; Wang, X. P.; Zhang, B. Y.; Zhu, J. G.; Xiao, D. Q.; Wang, X. J.; Lou, X. J.; Liang, W. F. Lead-free Piezoelectric Ceramics Based on (0.97-x)$K_{0.48}Na_{0.52}NbO_3$-0.03 $Bi_{0.5}(Na_{0.7}K_{0.2}Li_{0.1})_{0.5}ZrO_3$-$x$$B_{0.5}Na_{0.5}TiO_3$ Ternary System. *J. Appl. Phys.* **2013**, *114*, 124107.
(24) Zuo, R. Z.; Fang, X. S.; Ye, C. Phase Structures and Electrical Properties of New Lead-free ($Na_{0.5}K_{0.5}$)NbO_3−($Bi_{0.5}Na_{0.5}$)TiO_3 Ceramics. *Appl. Phys. Lett.* **2007**, *90*, 092904.
(25) Du, H.; Zhou, W.; Zhu, D.; Fa, L.; et al. Sintering Characteristic, Microstructure, and Dielectric Relaxor Behavior of ($K_{0.5}Na_{0.5}$)NbO_3−($Bi_{0.5}Na_{0.5}$)TiO_3 Lead-free Ceramics. *J. Am. Ceram. Soc.* **2008**, *91* (9), 2903−2909.
(26) Gou, Q.; Xiao, D.; Wu, B.; Xiao, M.; Feng, S.; Ma, Z.; Xiao, D. Q.; Zhu, J. G. New (1-x)$K_{0.5}Na_{0.5}NbO_3$−x(0.15 $Bi_{0.5}Na_{0.5}TiO_3$−0.85 $Bi_{0.5}Na_{0.5}ZrO_3$) Ternary Lead-free Ceramics: Microstructure and Electrical Properties. *RSC Adv.* **2015**, *5* (39), 30660−30666.
(27) Cross, L. E. Ferroelectric Materials for Electromechanical Transducer Applications. *Mater. Chem. Phys.* **1996**, *43*, 108−115.
(28) Zhang, S. T.; Kounga, A. B.; Aulbach, E.; Ehrenberg, H.; Rodel, J. Giant Strain in Lead-free Piezoceramics $Bi_{0.5}Na_{0.5}TiO_3$−$BaTiO_3$−$K_{0.5}Na_{0.5}NbO_3$ System. *Appl. Phys. Lett.* **2007**, *91*, 112906.
(29) Yan, K.; Ren, X. Multi-phase Transition Behaviour and Large Electrostrain in Lead-free (K, Na, Li) NbO_3 Ceramics. *J. Phys. D: Appl. Phys.* **2014**, *47*, 015309.
(30) Wu, J. G.; Tao, H.; Yuan, Y.; Lv, X.; Wang, X. J.; Lou, X. J.Role of Antimony in the Phase Structure and Electrical Properties of Potassium−Sodium Niobate Lead-free Ceramics. *RSC Adv.* **2015**, *5* (19), 14575−14583.
(31) Acker, J.; Kungl, H.; Hoffmann, M. J. Influence of Alkaline and Niobium Excess on Sintering and Microstructure of Sodium-Potassium Niobate ($K_{0.5}Na_{0.5}$)NbO_3. *J. Am. Ceram. Soc.* **2010**, *93* (5), 1270−1281.
(32) Liang, L. Y.; Li, Y. L.; Hu, S. Y.; Chen, L. Q.; Lu, G. H. Piezoelectric Anisotropy of a $KNbO_3$ Single Crystal. *J. Appl. Phys.* **2010**, *108*, 094111.

DOI: 10.1021/acsami.5b06033
ACS Appl. Mater. Interfaces 2015, 7, 20332−20341